Mon. Not. R. Astron. Soc. **000**, 1–11 (2014) Printed 18 September 2014 (MN LATEX style file v2.2)

Running with *BICEP*2: Implications for Small-Scale Problems in CDM

Shea Garrison-Kimmel[1⋆], Shunsaku Horiuchi[1,2], Kevork N. Abazajian[1], James S. Bullock[1], Manoj Kaplinghat[1]
[1] *Center for Cosmology, Department of Physics and Astronomy, University of California, Irvine, CA 92697, USA*
[2] *McCue Fellow*

arXiv:1405.3985v2 [astro-ph.CO] 17 Sep 2014

18 September 2014

ABSTRACT
The *BICEP*2 results, when interpreted as a gravitational wave signal and combined with other CMB data, suggest a roll-off in power towards small scales in the primordial matter power spectrum. Among the simplest possibilities is a running of the spectral index. Here we show that the preferred level of running alleviates small-scale issues within the ΛCDM model, more so even than viable WDM models. We use cosmological zoom-in simulations of a Milky Way-size halo along with full-box simulations to compare predictions among four separate cosmologies: a *BICEP*2-inspired running index model ($\alpha_s = -0.024$), two fixed-tilt ΛCDM models motivated by *Planck*, and a 2.6 keV thermal WDM model. We find that the running *BICEP*2 model reduces the central densities of large dwarf-size halos ($V_{\rm max} \sim 30 - 80\,{\rm km\,s^{-1}}$) and alleviates the too-big-to-fail problem significantly compared to our adopted *Planck* and WDM cases. Further, the *BICEP*2 model suppresses the count of small subhalos by $\sim 50\%$ relative to *Planck* models, and yields a significantly lower "boost" factor for dark matter annihilation signals. Our findings highlight the need to understand the shape of the primordial power spectrum in order to correctly interpret small-scale data.

Key words: dark matter – cosmology: theory – galaxies: halos – Local Group

1 INTRODUCTION

The discovery of the cosmic microwave background (CMB) and measurements of its temperature anisotropy have lead to a standard cosmological model consisting of a flat universe dominated by cold dark matter and a cosmological constant that drives accelerated expansion at late times (e.g., Planck Collaboration et al., 2013). Inflation extends this standard cosmology by positing an earlier period of rapid exponential expansion that sets the initial conditions for the hot big bang; this period alleviates a number of "fine-tuning" problems, but lacked supporting observational evidence. Recently, however, the *BICEP*2 experiment reported the detection of primordial B-modes in the CMB (BICEP2 Collaboration et al., 2014; Ade et al., 2014). One explanation for this signal is the stochastic background of gravitational waves generated by inflation, providing potentially the first direct evidence for an inflationary phase in the early Universe. This explanation will have to be verified by other experiments and in other frequencies. For the rest of this paper, we will assume this explanation is correct as we await confirmation by other experiments and in other frequency bands. [1]

The tensor-to-scalar ratio measured by *BICEP*2, $r = 0.20^{+0.07}_{-0.05}$ (68% confidence-interval), is at face value inconsistent with the limit quoted from a combination of *Planck* (Planck Collaboration et al., 2013; Ade et al., 2013), *SPT* (Hou et al., 2014), *ACT* (Das et al., 2014), and *WMAP* polarization (Hinshaw et al., 2013) data: $r < 0.11$ at 95% confidence.[2] However, these pre-*BICEP*2 limits assumed a constant spectral index n_s for scalar fluctuations in the primordial power spectrum. The discrepancy could be explained by a nontrivial primordial power spectrum, one that deviates from a pure power law (e.g., Hazra et al., 2014); suppressing the large-scale scalar power spectrum relative to that

[1] In this regard, note that there has been concern that foreground contamination could have affected this measurement (e.g. Liu et al., 2014).
[2] As noted by Audren et al. (2014), however, the measured tension may be significantly reduced ($\sim 1.3\sigma$) by assuming identical values for the pivot scale and the tensor spectral index in both analyses, effectively raising the upper limits on the running measured by *Planck*.

⋆ sgarriso@uci.edu

© 2014 RAS

expected in a constant spectral index model allows for a larger contribution from tensor modes to the temperature-temperature anisotropy C_l^{TT} at large scales . Abazajian et al. (2014) explored several scenarios including a running spectral index, a cutoff in the spectrum, and a break in the power spectrum, finding evidence for a negative running index (see also McDonald, 2014; Ashoorioon et al., 2014) or for a broken spectrum. Of these possibilities, the running spectral index is arguably the simplest, and we focus on the small-scale implications of this solution for the remainder of this work. More generally, however, our results explore the possible implications of non-trivial primordial power spectra on galaxy formation. Here we specifically show that viable deviations from power-law primordial power spectrum can have a significant impact on important questions facing ΛCDM today.

Any modifications to the primordial power spectrum and cosmological parameters will manifest itself in the formation and evolution of large-scale structure. On large scales, the standard ΛCDM cosmology provides an excellent model for the observed Universe (Ho et al., 2012; Hinshaw et al., 2013); any changes that compromise this success would thus be a sign of an inconsistent scenario.

On the other hand, discrepancies currently exist between the ΛCDM paradigm and the observed Universe on smaller scales. Examples include the "core/cusp problem," where dissipationless N-body simulations in ΛCDM predict a rising dark matter density with smaller radius $\rho \propto r^{-1}$, in contrast to observations that show a core-like profile at small radii (Flores & Primack, 1994; Moore et al., 1999). The discrepancy is seen in low-surface brightness (LSB) galaxies (Simon et al., 2005; Donato et al., 2009; de Naray & Kaufmann, 2011; Oh et al., 2011), but also seems to appear in lower luminosity dwarf spheroidal (dSph) galaxies [3] (Walker & Penarrubia, 2011; Agnello & Evans, 2012; Amorisco & Evans, 2012). A second discrepancy is that the count of known satellite galaxies around the Milky Way is much smaller than the count of subhalos expected to be massive enough to form stars (Klypin et al., 1999; Moore et al., 1999, the "missing satellites problem"). Independently, it has also been shown that the central densities of dSphs are significantly lower than predicted by dissipationless ΛCDM simulations, dubbed the "too-big-to-fail problem" (TBTF; Boylan-Kolchin et al., 2011, 2012). The severity of TBTF remains an active debate in the literature, with some authors pointing out that a reduced MW mass would effectively eliminate the problematic halos (e.g. Wang et al., 2012; Cautun et al., 2014) and others arguing that baryonic processes, such as reionization, supernovae feedback, tidal interactions, and ram pressure stripping, may reduce the central densities of simulated dwarf halos (e.g. Bullock et al., 2000; Somerville, 2002; Pontzen & Governato, 2012; Zolotov et al., 2012; Brooks & Zolotov, 2014; Arraki et al., 2013; Gritschneder & Lin, 2013; Garrison-Kimmel et al., 2013; Amorisco et al., 2014; Del Popolo et al., 2014; Sawala et al., 2014; Pontzen & Governato, 2014).

Quantitatively, the magnitude of these small-scale problems and the degree to which feedback and other baryonic processes can operate to solve them depend on the underlying power spectrum and cosmological parameters, which fundamentally affect the collapse times and central densities of dark matter halos. For example, Zentner & Bullock (2002, 2003) showed that non-trivial primordial power spectra of the type expected in basic inflation models can alleviate many of the small-scale problems faced by ΛCDM, and used semi-analytic models to show that running at the level of $\alpha_s \simeq -0.03$ can reduce discrepancies significantly. Later, using numerical simulations, Polisensky & Ricotti (2014) showed that differences in best-fit σ_8 and n_s values between WMAP data releases impact small-scale predictions in important ways. The implication is that changes that follow from the *BICEP*2 results can affect the magnitude of small-scale discrepancies significantly. Similarly, imposing a free-streaming cutoff in the initial power spectrum (e.g. from warm dark matter, WDM, or from a non-trivial inflation model) may also aid in resolving problems (Kamionkowski & Liddle, 2000; Zentner & Bullock, 2003; Kaplinghat, 2005; Lovell et al., 2014; Schneider et al., 2014). Specifically, WDM with a thermal mass of 2 keV has been shown to be sufficient to solve some of the problems (Anderhalden et al., 2013). Although this mass is in conflict with existing limits on free-streaming cutoffs (e.g., Polisensky & Ricotti, 2011; Viel et al., 2013; Schneider et al., 2014), the limits are subject to systematic uncertainties, and more robust limits based on phase-space arguments and subhalo counting are just below 2 keV (Boyarsky et al., 2009; Gorbunov et al., 2008; Horiuchi et al., 2014).

The *BICEP*2 measurement may also have interesting consequences on searches for potential annihilation signals from dark matter itself (indirect detection studies). The annihilation signal from a single halo scales as the square of the dark matter density, $\rho^2_{\rm DM}$ (Strigari et al., 2008), and the total "boost" factor, the contribution to the expected annihilation signal due to substructure, is dependent on the slope and normalization of the substructure mass function. Reducing any of these quantities could significantly loosen the upper limits placed by the searches that employ substructure boost (Kamionkowski et al., 2010; Anderson et al., 2010; Sánchez-Conde & Prada, 2014; Ng et al., 2014).

In this paper, we investigate the impact of the running power spectrum on structure formation in the Universe by simulating the evolution of a MW-size host in four separate cosmologies: the model motivated by *BICEP*2, the *Planck* cosmological model, a WDM model with the *Planck* parameter set, and a flat universe with a lowered $\Omega_{\rm m}$ but otherwise identical to the *Planck* universe in order to control for the difference in $\Omega_{\rm m}$ between the *Planck* and *BICEP*2 models.

This paper is organized as follows: § 2 describes the simulations, including the cosmological models that we compare; § 3 presents our results for the cosmological mass function at $z = 3$, the subhalo $V_{\rm max}$ function of a MW-size host at $z = 0$, and discuss the changes in the internal kinematics of the highest mass subhalos (the TBTF problem) as well as implications for the substructure boost; we summarize our findings in § 4.

[3] We note that the density profiles of dSphs are currently a matter of some debate (e.g. Breddels & Helmi, 2013).

Parameter	*BICEP*2	*Planck*	*Low*-$\Omega_{\rm M}$	$WDM_{2.6{\rm keV}}$
$\alpha_{\rm s}$	-0.024	0	0	0
h	0.698	0.6711	0.6711	0.6711
$\Omega_{\rm m}$	0.285	0.3175	0.26	0.3175
Ω_Λ	0.715	0.6825	0.74	0.6825
σ_8	0.835	0.8344	0.8344	0.8344
$n_{\rm s}$	0.967	0.9624	0.9624	0.9624
$m_{\rm WDM}$	—	—	—	2.6 keV
$m_{\rm p,\,HR}$	1.44	1.6	1.31	1.6
$m_{\rm p,\,FB}$	92.1	102.6	84	—

Table 1. The four sets of cosmological parameters used in this work. The first column indicates the parameter, the second lists the adopted *BICEP*2 cosmology from Abazajian et al. (2014), the third gives the parameters from *Planck* adopted here (taken from the temperature power spectrum; Planck Collaboration et al., 2013), the fourth column lists the "*Low*-$\Omega_{\rm M}$" cosmology, which is identical to the *Planck* parameter set but with an overall matter density below that suggested by *BICEP*2. The final column, which we refer to as "$WDM_{2.6{\rm keV}}$," is identical to the *Planck* cosmology, but includes a WDM free-streaming cut-off in the power spectrum for a thermal WDM particle mass of $m_{\rm WDM} = 2.6$keV (see Figure 1). Particle masses are given in units of $10^5 h^{-1}\,M_\odot$. $\alpha_{\rm s}$ is the running, defined in the text.

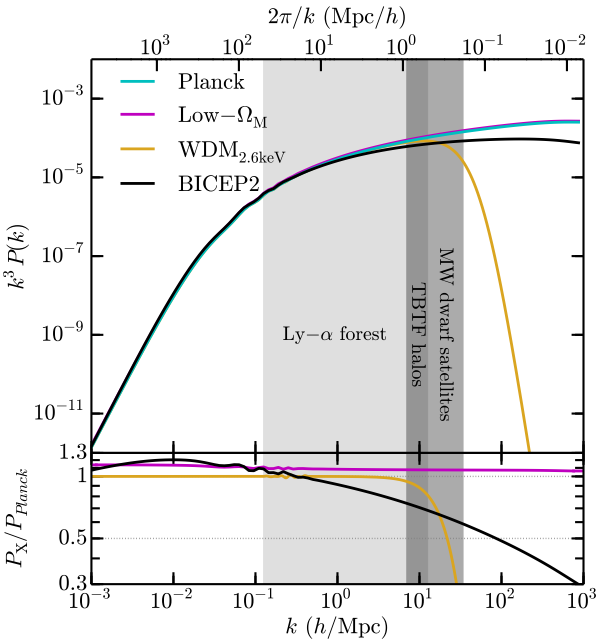

Figure 1. Top: The primordial power spectrum in the *BICEP*2 (black), *Planck* (cyan), $WDM_{2.6{\rm keV}}$ (yellow), and *Low*-$\Omega_{\rm M}$ (magenta) cosmologies adopted in this paper, used for creating the initial conditions for the simulations. Bottom: The ratio of the power spectra relative to that of *Planck*. The light shaded region in both panels indicates the regime that Viel et al. (2013) probe with the Lyman-α forest, where the *BICEP*2 power spectrum differs by $\lesssim 30\%$ and where that of $WDM_{2.6{\rm keV}}$ agrees nearly perfectly, until the sharp cutoff just below the smallest scales probed by Ly-α. On the mass scales relevant to small-scale galaxy formation ($M_{\rm halo} \sim 10^9 - 10^{11} h^{-1}\,M_\odot$, indicated in dark grey) however, *BICEP*2 differs by nearly a factor of 2 and $WDM_{2.6{\rm keV}}$ quickly falls off due to relativistic free-streaming in the early Universe. The overlap region roughly corresponds to the mass scales of halos characteristic of the too-big-to-fail problem. The *Low*-$\Omega_{\rm M}$ model is everywhere $\sim 10\%$ higher than the standard *Planck* model at $z = 125$ due to the constraint that the linear power spectra agree at $z = 0$.

2 SIMULATIONS AND ANALYSIS

We have run collisionless, dark matter-only simulations of a $50h^{-1}$ Mpc periodic region with the Tree-PM code `Gadget-3` (Springel, 2005), beginning at $z = 125$. We present seven simulations, three of which model the full volume at medium resolution ($n_{\rm p} = 1024^3$) and four of which are "zoom-in" simulations aimed at a Milky Way (MW)-size host. Initial conditions were created with `MUSIC` (Hahn & Abel, 2011). We include the running in the *BICEP*2 universe by defining

$$T'^2(k) = \left(\frac{k}{k_\star}\right)^{\frac{1}{2}\alpha_{\rm s}\ln\left(\frac{k}{k_\star}\right)} T^2(k), \qquad (1)$$

where $\alpha_{\rm s} = dn_{\rm s}/d\ln k$ is the running of the spectral index, $k_\star = 0.05\,{\rm Mpc}^{-1}$ (Abazajian et al., 2014), and $T(k)$ is the standard definition of the transfer function. We pass $T'^(k)$ to `MUSIC` as the transfer function.

We list the four underlying cosmological models that we adopt in Table 1. For the *BICEP*2 universe, we select the "running" model from Abazajian et al. (2014), who performed a joint Bayesian analysis on the *BICEP*2 *B*-mode polarization data and the temperature and lensing data from Planck Collaboration et al. (2013); those parameters are listed in the first column. We elect to compare this model to that suggested by the *Planck* temperature power spectrum data alone (Table 2, Column 2 of Planck Collaboration et al., 2013), reproduced in the second column. We additionally simulate structure formation in two *Planck*-like control models, *Low*-$\Omega_{\rm M}$ and $WDM_{2.6{\rm keV}}$. Both adopt the majority of the *Planck* parameters, but *Low*-$\Omega_{\rm M}$ artificially lowers the overall matter density, $\Omega_{\rm m}$, to $\sim 3\sigma$ below that suggested by Abazajian et al. (2014) (while maintaining flatness) in order to control for the lowered $\Omega_{\rm m}$ in the *BICEP*2 cosmology. The $WDM_{2.6{\rm keV}}$ cosmology is identical to the *Planck* model, but imposes a relativistic free-streaming cut-off in the power spectrum for a thermal WDM particle equivalent mass of $m_{\rm WDM} = 2.6$ keV. The mass is chosen to obey the robust limits from phase-space arguments of MW dSphs galaxies and strict counting of M31 satellites (Horiuchi et al., 2014), and is also marginally consistent with measurements of the Ly-α at 3σ (Viel et al., 2013). A WDM particle mass of 2 keV has been shown to solve small-scale issues in CDM (Anderhalden et al., 2013), but we opt for a slightly more massive particle in order to explore a value distinct from other works.

The initial ($z = 125$) matter power spectra for these cosmologies are shown in Figure 1. The upper panel plots $k^3P(k)$ for the *BICEP*2 parameters in black, the *Planck* model in cyan, and the *Low*-$\Omega_{\rm M}$ and $WDM_{2.6{\rm keV}}$ control models in magenta and yellow, respectively. The ratio of each model, relative to the *Planck* power spectrum is plotted in the lower panel. The light-grey region indicates the scales that are currently probed by the Lyman-α forest ($50h^{-1}\,{\rm Mpc} - 0.5h^{-1}\,{\rm Mpc}$; Viel et al., 2013) and the dark grey region indicates the mass ranges of interest to dwarf galaxy formation ($M_{\rm halo} \sim 10^9 - 10^{11} M_\odot$); the darkest overlap region roughly corresponds to the mass scales of $V_{\rm max} \sim 35\ {\rm km\,s^{-1}}$ halos, which are characteristic of the problematic halos identified in TBTF. The *BICEP*2 power

spectrum differs from that of *Planck* by as much as $\sim 30\%$ at the scales probed by the Ly-α forest; studies of the Ly-α forest power spectrum are sensitive to running, and the most recent results have found values consistent with the running we adopt here $\alpha_s = -0.028 \pm 0.018$ (Lesgourgues et al., 2007). The $\gtrsim 30\%$ reduction in the primordial power at the smaller scales associated with the formation of dwarf halos, however, has interesting consequences for the small-scale problems discussed above. The unlabeled region to the right of the dwarf scales are associated with so-called "mini-halos," which may be probed by gravitational lensing studies (e.g., Keeton & Moustakas, 2009) or tidal stream analyses (Ngan & Carlberg, 2014). This range is also important for the overall "boost" factor due to dark matter annihilation in substructure (Sánchez-Conde & Prada, 2014), indicating that the *BICEP*2 power spectrum will likely produce a much smaller DM annihilation signal from these mini-halos.

We first compare the cosmologies by simulating the entire 50 h^{-1} Mpc volume at moderate resolution ($n_{\rm p} = 1024^3$) until $z = 3$ with the *Planck*, *Low*-$\Omega_{\rm M}$, and *BICEP*2 cosmologies.[4] The particle masses for these "full-box" simulations are given in Table 1 as $m_{\rm p,\,FB}$ in units of $10^5 M_\odot$. We fix the Plummer-equivalent softening lengths of the full-box simulations at 5 comoving h^{-1} kpc until $z = 9$, at which time they become 500 physical h^{-1} pc. Dark matter structure is identified with the `AMIGA Halo Finder` (`AHF`; Knollmann & Knebe, 2009), a publicly-available three-dimensional spherical overdensity halo finder.[5] A slice of the simulation volume at $z = 3$ is shown in Figure 2 for the *BICEP*2 cosmology (top) and the fiducial *Planck* model (bottom) – the two appear indistinguishable at these scales, though we will show below that there is a small systematic offset in the halo mass function, consistent with expectations from linear theory.

In order to study the highly non-linear regime, however, we primarily focus our efforts on "zoom-in" simulations (Katz & White, 1993; Oñorbe et al., 2014) aimed at a MW-size host, similar to the Via Lactea II (Diemand et al., 2008; Kuhlen et al., 2008) and Aquarius (Springel et al., 2008) projects. Specifically, we selected a highly isolated host from the ELVIS simulations (Garrison-Kimmel et al., 2014a) and re-create the parent box, oversampling the region from which the halo forms with higher resolution, with the four underlying cosmological models given in Table 1. The zoom-in simulations are initialized with an effective resolution of 4096^3 particles in the high resolution region. Similar to the full-box simulations, the softening lengths of these lowest mass particles is kept fixed at 1 comoving h^{-1} kpc until $z = 9$, after which it is held fixed at 100 physical h^{-1} pc until $z = 0$. The particle masses for each cosmological model are listed as $m_{\rm p,\,HR}$ in Table 1, again in units of $10^5 h^{-1}\,M_\odot$. Each cosmological model was initialized with identical phases for the perturbations at all scales in order to reduce numerical differences (e.g., in the subhalo orbits) between the models. As in the full-box simulations, we search for collapsed structures in the $z = 0$ particle data with `AHF`.[6] A visualization of a cube 500 h^{-1} kpc on a side, centered on the zoom-in target, is shown in Figure 3. The images are colored by the local matter density and show, from top left to bottom right, the *BICEP*2 simulation, the *Planck* model, the *Low*-$\Omega_{\rm M}$ cosmology, and the $WDM_{\rm 2.6keV}$ model. The agreement between the *Planck* models, in spite of the free-streaming cutoff or shift in $\Omega_{\rm m}$, is uncanny; the *BICEP*2 cosmology, however, has less overall substructure and clearly distinct orbits for the largest subhalos, indicative of the significant differences in power at $M \sim 10^9 - 10^{11} M_\odot$ scales seen in Figure 1.

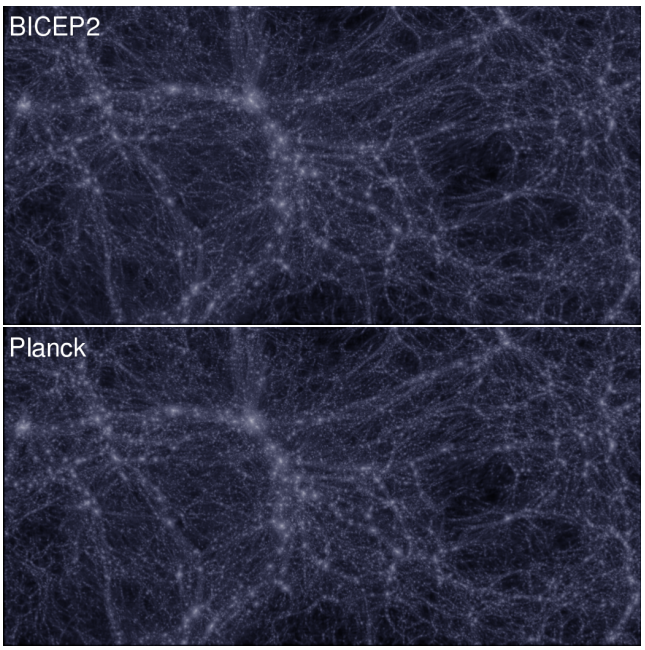

Figure 2. Visualizations of the large-scale dark matter density field at $z = 3$ in the *BICEP*2 (top) and *Planck* (bottom) cosmologies. Shown is a slab 25 h^{-1} Mpc wide, 12.5 h^{-1} Mpc tall, and 5 h^{-1} Mpc deep. The two matter fields initially appear indistinguishable on these scales, though we will show below that there are small differences in the halo mass function, which become even stronger on the scales of dwarf galaxies.

Our zoom-in simulations are run with identical particle numbers, box sizes, and softening lengths (in h^{-1} units) as the fiducial simulations in the ELVIS Suite (Garrison-Kimmel et al., 2014a); we therefore adopt the ELVIS resolution cut here and study only halos with maximum circular velocities $V_{\rm max} > 8$ km s^{-1}. Similarly, Garrison-Kimmel et al. (2014b) showed that the relationship between $V_{\rm max}$ and the radius at which $V_{\rm max}$ occurs, $R_{\rm max}$, is converged for halos larger than 15 km s^{-1} and with $R_{\rm max} > 0.36$ h^{-1} kpc for simulations at this resolution; we again use the same criteria when examining the internal structure of small halos.

3 RESULTS

We begin by examining the halo mass function in the 50 h^{-1} Mpc full-box runs at $z = 3$. Plotted as solid lines

[4] We do not simulate the volume with the $WDM_{\rm 2.6keV}$ cosmology as the model is designed to agree with our *Planck* run at the scales probed by such a simulation.

[5] `AHF` is available at `http://popia.ft.uam.es/AHF/Download.html`.

[6] We also find identical results using the 6D friend-of-friends halo finder `ROCKSTAR` (Behroozi et al., 2013).

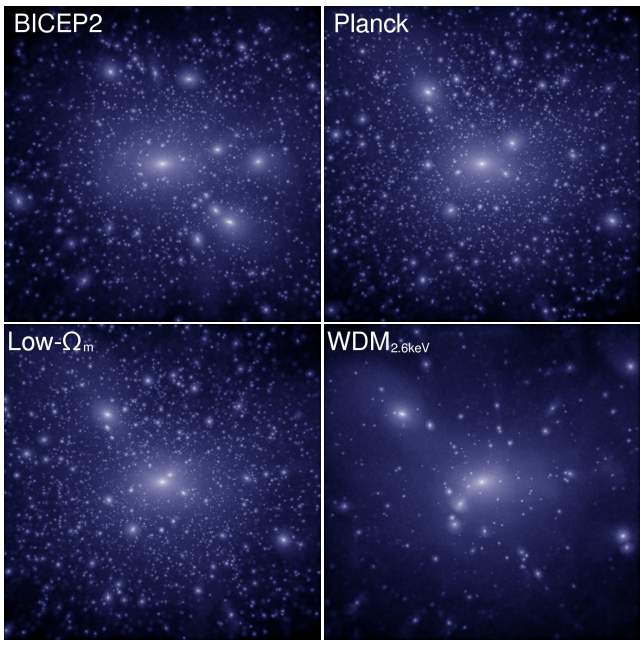

Figure 3. Visualizations of the zoom-in halo, colored by the local matter density, in the *BICEP*2 (top left), *Planck* (top right), *Low*-$\Omega_{\rm M}$ (bottom left), and *WDM*$_{2.6\rm keV}$ (bottom right) cosmologies. Shown are cubes 500 h^{-1} kpc on a side, centered on the targeted host. The relative lack of substructure in the *WDM*$_{2.6\rm keV}$ run and the agreement between the orbits of the largest halos between the *Planck* models are visible even by eye. The *BICEP*2 simulation, however, displays clearly different subhalo orbits and hints at reduced substructure at the smallest masses.

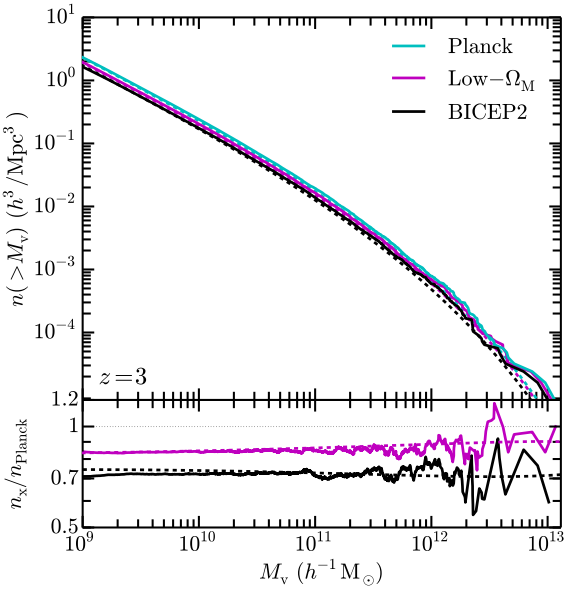

Figure 4. The anti-cumulative mass function, per unit volume, of all host halos in the 50 h^{-1} Mpc volume at $z = 3$ from the simulations (solid lines) and from applying the Tinker et al. (2008) analytical fitting function (dashed lines) for the *BICEP*2 (black), *Planck* (cyan) and *Low*-$\Omega_{\rm M}$ (magenta) models (upper panel) and the ratios of the *BICEP*2 and *Low*-$\Omega_{\rm M}$ models to the *Planck* model (lower panel). At fixed mass, the *BICEP*2 cosmology predicts $\sim 30\%$ fewer halos than the *Planck* model, consistent with expectations from linear theory. Alternatively, halo masses at fixed number counts are $\sim 20-30\%$ lower in the *BICEP*2 model, again compared to *Planck*.

in the top panel of Figure 4 is the anti-cumulative number density of host halos, defined as those with their centers outside the virial volumes [7] of all halos larger than itself, as a function of virial mass $M_{\rm v}$; the lower panel plots the ratio of each line relative to the fiducial *Planck* model. The *BICEP*2 cosmology exhibits a suppression on all mass scales such that the Planck mass function is offset by $\sim 30\%$ at fixed number, though the offset rises slighter at lower masses, consistent with the running in the power spectrum. We note that presenting results in $M_\odot$ rather than $h^{-1}\,M_\odot$ would only increase the difference between the two simulations as the *Planck* cosmology adopts a smaller Hubble parameter.

This offset, however, is consistent with expectations from linear theory of structure collapse. Plotted as dashed lines in Figure 4 are the results of applying the analytical fitting function of Tinker et al. (2008); [8] the ratios of these fitting functions are plotted as dashed lines in the lower panel. The Tinker et al. fit agrees nearly perfectly with our simulated mass functions, and the relative offsets from the *Planck* model are also in excellent agreement with the simulations. We conclude that analytic mass functions based on linear theory may be used to make accurate predictions (at least until $z = 3$) in the *BICEP*2 cosmology.

Given that the differences in the primordial power spectrum increase with decreasing scales, we can expect to see even more extreme differences on the scales of dwarf galaxy halos. We therefore turn our analysis to the zoom-in simulations described in Section 2, which we exclusively use for the remainder of the work. The properties of the main host halo, given in Table 2, vary slightly between the four models; we therefore present subhalo counts as a function of $V_{\rm max}/V_{\rm v}$, where $V_{\rm v}$ is the circular velocity of the host halo at the virial radius. This minimizes the halo-to-halo scatter and normalizes for the effects of varying host mass.

This normalized $V_{\rm max}$ function is plotted in the top panel of Figure 5 for all four cosmological models; the lower panel again plots the ratio of each model to the *Planck* cosmology. The upper axis is scaled to $V_{\rm v} = 160\,{\rm km\,s^{-1}}$, roughly the virial velocity of a MW-size host and the mean $V_{\rm v}$ of the host in the four simulations. When normalizing by $V_{\rm v}$, the agreement between the *Planck* and *Low*-$\Omega_{\rm M}$ models is nearly perfect at all $V_{\rm max}/V_{\rm v}$, even at the high $V_{\rm max}$ end where small-number statistics typically dominate; if the counts are not normalized by the virial velocity, however, the *Low*-$\Omega_{\rm M}$ model lies $\sim 25\%$ below the Planck cosmology at fixed subhalo $V_{\rm max}$. The *BICEP*2 counts, however, are suppressed even after normalizing by $V_{\rm v}$, particularly for subhalos less massive than $V_{\rm max} \sim 30\ {\rm km\,s^{-1}}$. The total count is $\sim 50\%$ below the *Planck* line at the resolution limit, alleviating the

[7] We use the term "virial radius" to refer to the radius at which the overdensity relative to the critical density drops to 173.8 (*BICEP*2), 174.3 (*Planck*), and 173.3 (*Low*-$\Omega_{\rm M}$) at $z = 3$ and 99.8 (*BICEP*2), 104.1 (*Planck*), 96.5 (*Low*-$\Omega_{\rm M}$), and 104.1 (*WDM*$_{2.6\rm keV}$) at $z = 0$, and "virial mass" to refer to the total mass contained within that radius.

[8] Theoretical mass functions are calculated via the publicly available code provided by Murray et al. (2013).

	$M_{\rm v}$ ($10^{12}\ h^{-1}\,M_\odot$)	$R_{\rm v}$ ($h^{-1}\,{\rm kpc}$)	$V_{\rm max}$ (${\rm km\,s^{-1}}$)	$V_{\rm v}$ (${\rm km\,s^{-1}}$)	$N_{\rm h}(<R_{\rm v})$ [>8 ${\rm km\,s^{-1}}$]	$N_{\rm p}(<R_{\rm v})$	$r_{\rm uncontam}$ ($h^{-1}\,{\rm Mpc}$)	$N_{\rm h}(<1\,h^{-1}\,{\rm Mpc})$ [>15 ${\rm km\,s^{-1}}$]
BICEP2	1.26	221	164	156	460	8.8×10^6	1.27	125
Planck	1.49	231	187	166	944	9.4×10^6	1.04	216
Low-$\Omega_{\rm M}$	1.21	222	176	153	709	9.3×10^6	1.05	166
$WDM_{2.6{\rm keV}}$	1.49	231	194	167	119	9.4×10^6	0.97	76

Table 2. The properties of the main host halo in the zoom-in simulations. In order, the columns are the virial mass $M_{\rm v}$, virial radius $R_{\rm v}$, maximum circular velocity $V_{\rm max}$, virial velocity $V_{\rm v}=\sqrt{GM_{\rm v}/R_{\rm v}}$, the number of resolved ($V_{\rm max}>8$ ${\rm km\,s^{-1}}$) subhalos within the virial radius $N_{\rm h}(<R_{\rm v})$, the number of simulation particles within the virial radius $N_{\rm p}$, the distance to the nearest low resolution particle $r_{\rm uncontam}$, and the number of halos with resolved internal structure ($V_{\rm max}>15$ ${\rm km\,s^{-1}}$) within 1 h^{-1} Mpc, $N_{\rm h}(<1\ h^{-1}\,{\rm Mpc})$.

severity of the missing satellites problem. As expected, subhalos are even more strongly suppressed in the $WDM_{2.6{\rm keV}}$ universe, with counts a factor of ~ 6 lower than the fiducial *Planck* model at the resolution limit. While this suppression drastically reduces the severity of the missing satellites problem, it may actually under-produce the required subhalo count compared to the known count of M31 satellite galaxies (e.g. Horiuchi et al., 2014).[9] The *BICEP2* model has no such difficulties.

Due to the overall suppression of substructure in *BICEP2* it is possible that counts of high mass ($V_{\rm max}\sim 80$ ${\rm km\,s^{-1}}$) satellites will provide an additional constraint on the running. While we do not see any significant differences in the few subhalos that exist in the simulated host at that mass range, it is possible that some reduction exists on a statistical level, particularly for close pairs. As Tollerud et al. (2011) showed that ΛCDMlike cosmologies reproduce observations reasonably well at Large Magellanic Cloud (LMC)-like masses, such counts may be used as a probe of the initial power spectrum in the future. Such a study, however, would require large simulations with higher resolution than those presented here, simulated until $z=0$.

We now turn our attention to the internal structure of the subhalos. The simulations used in this work do not fully resolve density profiles in the innermost ~ 500 pc of dwarf halos, but integral properties such as $V_{\rm max}$ and $R_{\rm max}$ are converged for $V_{\rm max}>15$ ${\rm km\,s^{-1}}$ objects. These two quantities fully define the two-parameter Navarro-Frenk-White (NFW; Navarro et al., 1996) density profile

$$\rho(r)=\frac{\rho_{\rm s}}{(r/r_{\rm s})(1+r/r_{\rm s})^2}, \qquad (2)$$

where $r_{\rm s}=R_{\rm max}/2.1626$ is a characteristic scale radius and $\rho_{\rm s}=\rho_{\rm s}(R_{\rm max},V_{\rm max})$ is four times the density at $r=r_{\rm s}$. We may therefore extrapolate a unique circular velocity curve into the inner regions of the halos to make predictions regarding the central densities and compare with observations at small radii. This extrapolation assumes that the inner structure of subhalos is not strongly dependent on cosmology (i.e. that subhalos still follow NFW profiles in *BICEP2*); for $WDM_{2.6{\rm keV}}$ at least, this extrapolation seems to be valid (Dunstan et al., 2011), but we note that varying the density profile can strongly impact the number of massive failures (Di Cintio et al., 2013; Garrison-Kimmel et al., 2014b). Similarly, we may predict the relative change in the annihilation signal from substructure by knowing only the relationship between $V_{\rm max}$ and $R_{\rm max}$, as the signal from a single halo or subhalo is proportional to $\rho_{\rm s}^2 r_{\rm s}^3$ (Strigari et al., 2008).

We thus begin our investigation by presenting this relationship for subhalos of the main host (within 300 physical kpc, for comparison to the MW satellites) in the four

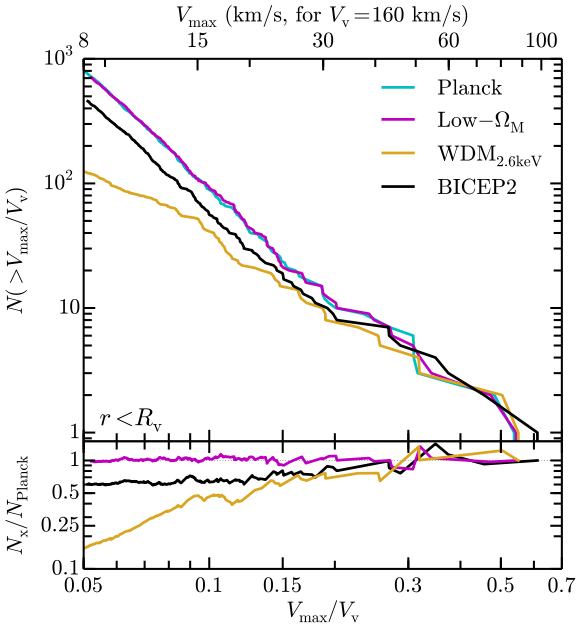

Figure 5. The anti-cumulative count of subhalos ($r<R_{\rm v}$) as a function of $V_{\rm max}$ normalized by the host virial velocity, $V_{\rm v}$ (upper panel) and the ratio of each cosmology to the *Planck* model (lower panel). Counts in the *Low-*$\Omega_{\rm M}$ cosmology (magenta line) match up nearly exactly with those in the standard *Planck* cosmology (cyan line), even though the host halo is $\sim 20\%$ less massive due to the modification in $\Omega_{\rm m}$. Counts in the *BICEP2* cosmology (black line), however, are systematically low for $V_{\rm max}/V_{\rm v}\lesssim 0.25$ ($V_{\rm max}\lesssim 40$ ${\rm km\,s^{-1}}$) and predict $\sim 50\%$ fewer halos at the resolution limit. The $WDM_{2.6{\rm keV}}$ model, meanwhile, drastically under-produces subhalos at low masses. Therefore, both the $WDM_{2.6{\rm keV}}$ and the *BICEP2* model will alleviate the missing satellites problem, though $WDM_{2.6{\rm keV}}$ may eliminate too many subhalos to explain, e.g., the observed satellite mass function of M31 (Horiuchi et al., 2014). The top axis is scaled to $V_{\rm v}=160$ ${\rm km\,s^{-1}}$, the mean virial velocity of the host in the four simulations.

[9] WDM N-body simulations are known to suffer from artificial fragmentation on small scales, leading to a non-negligible contribution to the halo catalog from spurious objects (e.g. Wang & White, 2007; Lovell et al., 2014). We do not explicitly account for this effect, which would act to suppress counts of small halos even further.

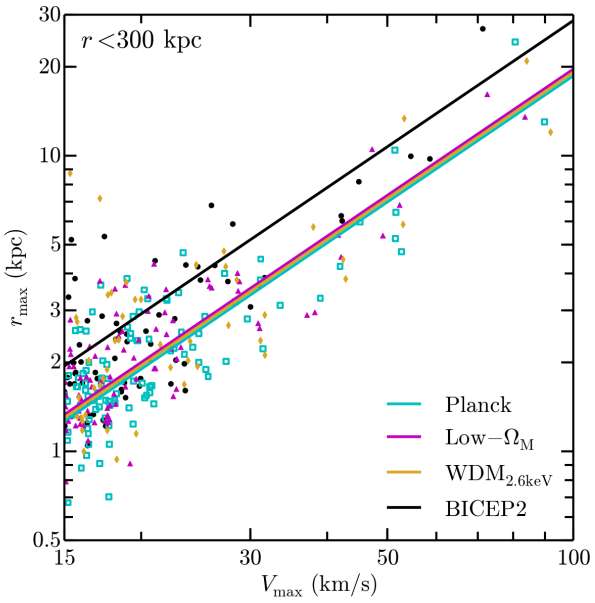

Figure 6. The relationship with $R_{\rm max}$ and $V_{\rm max}$ for subhalos in the *BICEP*2 (black circles), *Planck* (cyan squares), *Low*-$\Omega_{\rm M}$ (magenta triangles), and $WDM_{2.6{\rm keV}}$ (yellow diamonds) cosmologies, along with power-law fits to the data (Equation 3). The fits are weighted by $V_{\rm max}$ with the log-slope held fixed at the best-fit value in the *Planck* model, $p = 1.419$ (though there are weak indications that the slope is steeper in the *BICEP*2 model). The best-fit normalization in the *BICEP*2 cosmology is 35% lower than in the *Planck* simulation. In addition to helping to alleviate TBTF (see Figure 7), this overall shift in $R_{\rm max}$ at fixed $V_{\rm max}$ also implies a $\sim$ 35% lower annihilation signal from each subhalo in *BICEP*2. The normalizations, A, are 0.71 (*Planck*), 0.75 (*Low*-$\Omega_{\rm M}$), 0.73 ($WDM_{2.6{\rm keV}}$), and 1.09 (*BICEP*2).

cosmological models. Plotted in Figure 6 are the individual $R_{\rm max} - V_{\rm max}$ values for subhalos in each model, with the *BICEP*2 model plotted as black circles, the *Planck* model in cyan squares, the *Low*-$\Omega_{\rm M}$ model as magenta triangles, and the $WDM_{2.6{\rm keV}}$ model as yellow diamonds. The lines plot power-law fits to the subhalos:

$$\frac{R_{\rm max}}{1\ {\rm kpc}} = A\left(\frac{V_{\rm max}}{10\ {\rm km\,s^{-1}}}\right)^{p}. \qquad (3)$$

The contribution to the least-squares fit from each halo is weighted by the $V_{\rm max}$ of that halo to account for the scarcity of high $V_{\rm max}$ halos, and the log-slope p is held fixed at the value that best fits the data in the *Planck* cosmology, $p = 1.419$, allowing the normalization A to vary. [10] The three *Planck*-like models agree nearly perfectly: the normalizations differ by only 5%. The *BICEP*2 model, however, is clearly offset from the remaining three cosmologies with a normalization 35% higher.

It is interesting to note that the $WDM_{2.6{\rm keV}}$ model yields similar subhalo structural parameters ($V_{\rm max}$ - $R_{\rm max}$) to those of the *Planck* models, at least for the velocity range plotted here. Below we show that this is *not* the case for field halos in $WDM_{2.6{\rm keV}}$, which are less concentrated than *Planck* halos in the field. We interpret this differences as an effect of enhanced subhalo stripping for the $WDM_{2.6{\rm keV}}$ subhalos. Host halos tend to strip matter from the outer parts of subhalos, making them more concentrated with time. The $WDM_{2.6{\rm keV}}$ host halo density and mass remain similar to that in *Planck* cosmology, and the relative stripping experienced by the low-concentration infalling subhalos is more significant than it is in any of the other models. This is also consistent with the fact that we see many fewer subhalos in the $WDM_{2.6{\rm keV}}$ case.

The differences seen in Figures 5 and 6 impact the counts of discrepant TBTF halos. We directly compare the circular velocity curves predicted for each of our runs to observations of the classical MW dwarf spheroidal (dSphs) galaxies in Figure 7 – each line represents a single subhalo within 300 kpc and each point indicates a MW satellite. The left panel plots the *Planck* model, the central panel indicates the results in $WDM_{2.6{\rm keV}}$, and the right panel plots subhalos in the adopted *BICEP*2 cosmology. As in Boylan-Kolchin et al. (2011, 2012), the observational sample is comprised of the galaxies within 300 kpc of the MW with $L > 10^5\ L_{\odot}$, excluding the Magellanic Clouds and the Sagittarius dwarf. The former is removed from the sample because satellites as large as the Clouds are rare around MW-size hosts (Boylan-Kolchin et al., 2010; Busha et al., 2011; Tollerud et al., 2011); we remove the latter because it is currently interacting with the MW disk and is therefore not in equilibrium. For the remaining dwarfs, we plot $V_{1/2}$ at $r_{1/2}$, the circular velocity at the half-light radius, with 1σ errors in Figure 7. The values are taken from Wolf et al. (2010), who used data from Walker et al. (2009), Muñoz et al. (2005), Koch et al. (2007), Simon & Geha (2007) and Mateo et al. (2008).

The lines in Figure 7 each indicate an NFW rotation curve for a single subhalo of the central host. The dashed lines indicate the simulated analogs to the Magellanic Clouds, defined here as subhalos with $V_{\rm max} > 60\ {\rm km\,s^{-1}}$, which we remove from our analysis and plot only for illustrative purposes. The dotted lines indicate circular velocity profiles that fall below the 1σ error on $V_{1/2}$ for at least one of the MW dSphs – these subhalos are nominally consistent with the observational data and can host a MW satellite. The solid lines, however, have circular velocities that lie above *all* the dSphs and therefore qualify as "massive failures" – subhalos without observational counterparts. Nearly all of these massive failures are large enough, even today, to have formed stars in the presence of an ionizing background (Bullock et al., 2000; Somerville, 2002; Sawala et al., 2014).

Though the TBTF problem remains evident in all three models plotted here, [11] the number of massive failures is noticeably reduced in the *BICEP*2 cosmology relative to the *Planck* model. Perhaps surprisingly, the running power spectrum of *BICEP*2 eliminates more massive failures than the chosen WDM free-streaming cutoff.[12] Moreover, the remaining massive failures in the *BICEP*2 model lie well below

[10] We have also tested a quadratic fit in log-space and do not find evidence for a roll-off at small $V_{\rm max}$, though there are weak indications that the slope is steeper for the *BICEP*2 subhalos.

[11] Though we do not plot it, the central halo in the *Low*-$\Omega_{\rm M}$ cosmology hosts eight massive failures.

[12] Though a lighter WDM mass will be more effective (e.g., Schneider et al., 2014), it is constrained by the Ly-α forest (Viel et al., 2013) and subhalo counting (Polisensky & Ricotti, 2011);

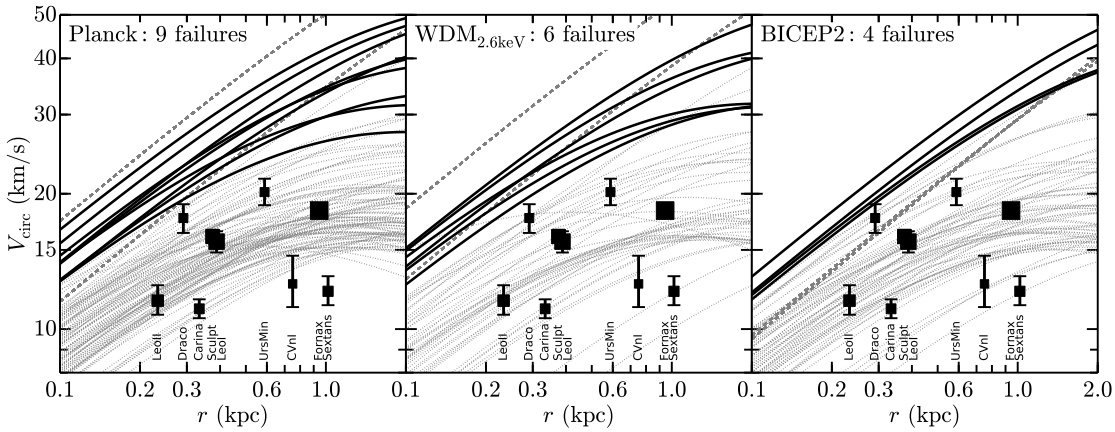

Figure 7. The rotation curves of all halos within 300 kpc of the host center with $V_{\rm max} > 15$ km s^{-1}, the smallest scale at which $R_{\rm max}$ can be reliably measured, in the *Planck* cosmology (left), the $WDM_{2.6\rm keV}$ model (center), and the adopted *BICEP*2 cosmology (right). The curves are extrapolated from $R_{\rm max}$ and $V_{\rm max}$ (Figure 6) by assuming an NFW profile. Also plotted are the constraints on the circular velocity at the half-light radius of the nine classical MW dwarfs used to define the TBTF problem in Boylan-Kolchin et al. (2011, 2012) from Wolf et al. (2010). Plotted as solid lines are those halos identified as massive failures – subhhalos that lie above the 1σ constraints on the MW dwarfs and thus cannot host any of the known bright satellites. As expected from Figure 6, which shows that subhalos in the *BICEP*2 cosmology are less dense at fixed $V_{\rm max}$ than in either the *Planck* or the $WDM_{2.6\rm keV}$ models, the problem is significantly alleviated (though not eliminated) by switching to the *BICEP*2 cosmology. For comparison, we note that the same halo contains eight massive failures in the *Low*-$\Omega_{\rm M}$ model.

the equivalent curves in the *Planck* cosmology, which acts to increase the efficacy of other processes (e.g. supernovae feedback) that may further reduce the central densities. Similarly, the *BICEP*2 cosmology significantly lowers the number of subhalos that are consistent with only Draco and Ursa Minor, the two highest density galaxies in the sample. Overall, the *BICEP*2 cosmology significantly reduces the magnitude of the TBTF problem, even without invoking baryonic processes that may further reduce the central densities (e.g. Zolotov et al., 2012), perhaps in a cosmology-dependent manner.

In addition to reducing the number of massive failures, the increase in $R_{\rm max}$ at fixed $V_{\rm max}$ in the *BICEP*2 cosmology implies a reduction in the substructure boost, i.e., the expected dark matter annihilation signal from subhalos. As noted above, the signal from a single halo scales as $\rho_{\rm s}^2 r_{\rm s}^3 \propto V_{\rm max}^4/R_{\rm max}$. Therefore, an increase of 35% in $R_{\rm max}$ at fixed $V_{\rm max}$ directly results in a 35% reduction in the annihilation signal. Furthermore, the overall boost is obtained by summing the signal from all the substructure by integrating the mass (or $V_{\rm max}$) function to masses well below $M_\odot$ (Martinez et al., 2009); assuming that the $\sim 50\%$ offset in the $V_{\rm max}$ function at the resolution limit ($V_{\rm max} = 8$ km s^{-1}) remains constant at lower masses, this implies that the substructure boost in the *BICEP*2 cosmology may be a factor of ~ 5 lower than in *Planck*. Moreover, the increasing roll-off of $P(k)$ at small scales implies that the relative offsets in both the $V_{\rm max}$ function and the $R_{\rm max} - V_{\rm max}$ relationship are even larger at small masses; the estimate will realistically be larger than 5.

For subhalos, the $R_{\rm max} - V_{\rm max}$ relation is due to a combination of the concentration-mass relationship at the time of formation and tidal stripping after infall onto the central host (Bullock et al., 2001; Ludlow et al., 2014). To more directly probe the former, Figure 8 plots $R_{\rm max}$ and $V_{\rm max}$ for halos in the field surrounding the central host, along with power-law fits (Equation 3) with p again held fixed at best fit value in the *Planck* simulation, $p = 1.26$. We limit ourselves to objects at least 500 kpc from the central host to avoid the majority of "backsplash" galaxies that have interacted with the host in the past (Teyssier et al., 2012; Garrison-Kimmel et al., 2014a), which may have undergone significant tidal stripping, and we select halos within 1.5 Mpc to avoid high mass (low resolution) contaminating particles.

While the agreement between the *Planck* and *Low*-$\Omega_{\rm M}$ models remains in the field (as expected due to their similar power spectra), the effects of the modifications to $P(k)$ are apparent in both the $WDM_{2.6\rm keV}$ and *BICEP*2 simulations. The latter two display significantly lower density halos, consistent with the suppression in power spectra at the time of formation; the fits to both are $\sim 50\%$ higher than the fit in the *Planck* cosmology. The most massive nearby field halo in the *BICEP*2 simulation is undergoing a major merger, resulting in an anomalously large $R_{\rm max}$ and we therefore perform the fit with and without that object. Including it results in the fit plotted as a black dashed line; the fit without that point is plotted as a solid black line.

4 CONCLUSIONS

We have tested the impact of the suppressed small-scale primordial power spectrum suggested by the recent *BICEP*2 results by simulating structure formation both with the "running" power spectrum suggested by these results and with the cosmology suggested by the *Planck* experiment, and using two control models – the *Planck* model with a free-

as discussed in Section 1, however, these constraints are subject to systematic uncertainties that are currently difficult to quantify.

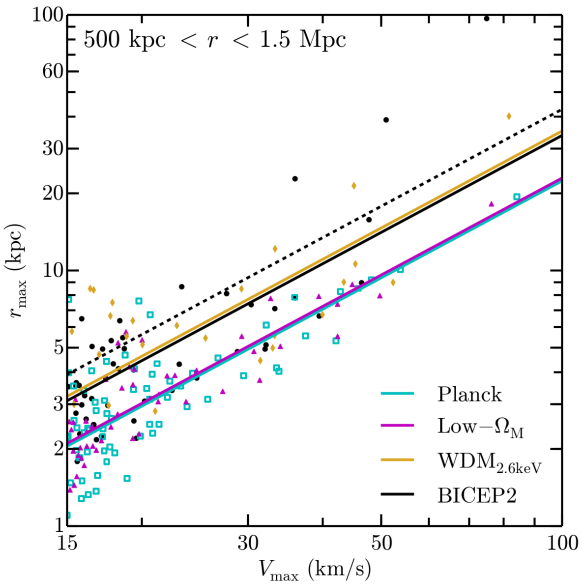

Figure 8. The $R_{\rm max}$-$V_{\rm max}$ relation for halos in the fields around the zoom-in target. Solid lines again plot fits (Equation 3) weighted by $V_{\rm max}$, with the log-slope again held fixed at the best-fit value for *Planck*, $p = 1.26$. The normalizations, A, are 1.23 (*Planck*), 1.26 (*Low*-$\Omega_{\rm M}$), 1.93 ($WDM_{2.6{\rm keV}}$), and 1.85 (*BICEP*2) – suppression in $P(k)$ at small scales in $WDM_{2.6{\rm keV}}$ and *BICEP*2 results in normalizations $\sim 50\%$ lower. The most massive halo in the *BICEP*2 field is excluded from the fit because the anomalously high $R_{\rm max}$ is due to an ongoing merger – including that halo results in a 20% larger normalization ($A = 2.35$), which is plotted as a black dashed line.

streaming cut-off corresponding to a WDM particle mass of 2.6 keV (thermal) and the *Planck* power spectrum with an artificially lowered $\Omega_{\rm m}$. We have simulated the evolution of identical $(50\ h^{-1}\,{\rm Mpc})^3$ volumes from $z = 125$ until $z = 3$ and the formation of a MW-size host until $z = 0$ at high resolution. These simulations indicate that the suppression in the primordial power spectrum at small scales results in mild offsets in the large-scale halo mass function (consistent with expectations from linear theory) and non-trivial differences in the subhalo $V_{\rm max}$ function and the inner structure of both field and satellite halos. Specifically:

- The $V_{\rm max}$ function of subhalos around a MW-size host in the *BICEP*2 cosmology lies well below that of the same host in the *Planck* model for $V_{\rm max} \lesssim 40\ {\rm km\,s^{-1}}$, even after normalizing for the differing sizes of the hosts. There are twice as many resolved ($V_{\rm max} > 8\ {\rm km\,s^{-1}}$) subhalos within the virial radius of the central host in the *Planck* simulation as result in the *BICEP*2 cosmology. The *Planck* and *Low*-$\Omega_{\rm M}$ models agree after scaling for the host mass. Unsurprisingly, the $WDM_{2.6{\rm keV}}$ simulation results in only $\sim 10\%$ as much substructure as our fiducial *Planck* run.
- Although masses of the largest subhalos around our selected host appear to be mostly unaffected by the changes in cosmology, the average concentrations (quantified here by the relationship between $R_{\rm max}$ and $V_{\rm max}$) of subhalos are significantly lower in the *BICEP*2 cosmology than any of the *Planck*-like models and our $WDM_{2.6{\rm keV}}$ run. This increase in $R_{\rm max}$ at fixed $V_{\rm max}$ alleviates the too-big-to-fail problem, and may increase the efficacy of baryonic processes that could further reduce the central densities.
- Taken together, the above two results imply that the substructure "boost," the contribution to the dark matter annihilation signal due to subhalos, is at least a factor of ~ 5 times smaller in the *BICEP*2 cosmology. Although the absolute value of the boost depends on many assumptions and is an uncertain quantity, this relative modification should be more robust and will work to lower previous upper limits to order unity.

While the above conclusions are drawn from simulations of only a single MW-size host halo, the overall trends demonstrated should hold for all such systems. Though there is significant scatter between MW-size systems (e.g. Boylan-Kolchin et al., 2010), the relative offset from the mean in the substructure population of a single host appears to remain largely static across cosmologies (Horiuchi et al., 2014). Therefore, the precise magnitude of the above changes may vary, but the general result that subhalos are less numerous and less dense in the *BICEP*2 model compared to *Planck* is robust. In order to accurately determine the range of substructure suppression and changes in concentration, one requires a large sample of simulations similar to those shown here; we elect to instead illustrate the general trends only.

Our results indicate that the level of spectral index running that reconciles the *BICEP*2 measurement with other constraints has interesting effects on dark matter structure over a range of scales. These changes are most evident at the smallest scales, where they help to alleviate small-scale issues with CDM. Though not addressed here, this type of reduction in small-scale power could have interesting implications for understanding cosmic reionization, which may require the early collapse of small halos and thus a fair amount of power on $\sim 10^8 M_\odot$ scales (e.g. Somerville et al., 2003; Robertson et al., 2013), and conversely studies of the early Universe may constrain the allowed running (similar to the constraints placed on WDM by Schultz et al., 2014). Signs of a non-trivial primordial power spectrum may also be explored in the Ly-α forest.

While it should be noted that inflationary models with precisely constant running at the level we have investigated have difficulty producing enough e-foldings (Easther & Peiris, 2006) and likely have higher order corrections to the power spectrum in this parameterization (Abazajian et al., 2005), there are feasible models with scale-dependent running that produce similar suppression of power at dwarf scales to that considered here (e.g., Kobayashi & Takahashi, 2011; Wan et al., 2014). The broad point of this work is to highlight the salient role that a non-trivial primordial power spectrum has in affecting small-scale predictions in ΛCDM. In light of the exciting *BICEP*2 results interpreted as evidence for inflationary gravitational waves, the need to consider non-standard primordial power spectra in structure formation studies has grown all the more urgent.

Acknowledgments
The authors thank Quinn Minor, Mike Boylan-Kolchin, Amjad Ashoorioon, Daniel Figueroa, and particularly the anonymous referee for helpful comments. SGK and JSB were

partially supported by NSF grants AST-1009973 and AST-1009999. SH is supported by the JSPS fellowship for research abroad, KA is supported by NSF CAREER Grant No. PHY-11-59224, and MK is supported by NSF Grant Nos. PHY-1214648 and PHY-1316792.

We also acknowledge the computational support of the NASA Advanced Supercomputing Division and the NASA Center for Climate Simulation, upon whose *Pleiades* and *Discover* systems the simulations were run, and the *Greenplanet* cluster at UCI, upon which much of the secondary analysis was performed. This research has made use of NASA's Astrophysics Data System.

References

Abazajian K., Kadota K., Stewart E. D., 2005, JCAP, 0508, 008
Abazajian K. N., Aslanyan G., Easther R., Price L. C., 2014, arXiv:1403.5922 [astro-ph]
Ade P., et al., 2013, arXiv:1303.5082 [astro-ph]
Ade P. A. R. et al., 2014, Physical Review Letters, 112, 241101
Agnello A., Evans N. W., 2012, ApJ, 754, L39
Amorisco N. C., Evans N. W., 2012, MNRAS, 419, 184
Amorisco N. C., Zavala J., de Boer T. J. L., 2014, ApJ, 782, L39
Anderhalden D., Schneider A., Macciò A. V., Diemand J., Bertone G., 2013, J. Cosmology Astropart. Phys., 3, 14
Anderson B., Kuhlen M., Diemand J., Johnson R. P., Madau P., 2010, ApJ, 718, 899
Arraki K. S., Klypin A., More S., Trujillo-Gomez S., 2013, MNRAS
Ashoorioon A., Dimopoulos K., Sheikh-Jabbari M. M., Shiu G., 2014, arXiv: 1403.6099 [hep-th]
Audren B., Figueroa D. G., Tram T., 2014, arXiv: 1405.1390 [astro-ph]
Behroozi P. S., Wechsler R. H., Wu H.-Y., 2013, ApJ, 762, 109
BICEP2 Collaboration et al., 2014, arXiv:1403.4302 [astro-ph]
Boyarsky A., Ruchayskiy O., Iakubovskyi D., 2009, J. Cosmology Astropart. Phys., 0903, 005
Boylan-Kolchin M., Bullock J. S., Kaplinghat M., 2011, MNRAS, 415, L40
Boylan-Kolchin M., Bullock J. S., Kaplinghat M., 2012, MNRAS, 422, 1203
Boylan-Kolchin M., Springel V., White S. D. M., Jenkins A., 2010, MNRAS, 406, 896
Breddels M. A., Helmi A., 2013, A&A, 558, A35
Brooks A. M., Zolotov A., 2014, ApJ, 786, 87
Bullock J. S., Kolatt T. S., Sigad Y., Somerville R. S., Kravtsov A. V., Klypin A. A., Primack J. R., Dekel A., 2001, MNRAS, 321, 559
Bullock J. S., Kravtsov A. V., Weinberg D. H., 2000, ApJ, 539, 517
Busha M. T., Wechsler R. H., Behroozi P. S., Gerke B. F., Klypin A. A., Primack J. R., 2011, ApJ, 743, 117
Cautun M., Frenk C. S., van de Weygaert R., Hellwing W. A., Jones B. J. T., 2014, arXiv: 1405.7697 [astro-ph]
Das S. et al., 2014, J. Cosmology Astropart. Phys., 4, 14
de Naray R. K., Kaufmann T., 2011, MNRAS, 414, 3617
Del Popolo A., Lima J. A. S., Fabris J. C., Rodrigues D. C., 2014, J. Cosmology Astropart. Phys., 4, 21
Di Cintio A., Knebe A., Libeskind N. I., Brook C., Yepes G., Gottlöber S., Hoffman Y., 2013, MNRAS, 431, 1220
Diemand J., Kuhlen M., Madau P., Zemp M., Moore B., Potter D., Stadel J., 2008, Nature, 454, 735
Donato F. et al., 2009, MNRAS, 397, 1169
Dunstan R. M., Abazajian K. N., Polisensky E., Ricotti M., 2011, arXiv: 1109.6291 [astro-ph]
Easther R., Peiris H. V., 2006, J. Cosmology Astropart. Phys., 9, 10
Flores R. A., Primack J. R., 1994, ApJ, 427, L1
Garrison-Kimmel S., Boylan-Kolchin M., Bullock J. S., Kirby E. N., 2014b, arXiv:1404.5313 [astro-ph]
Garrison-Kimmel S., Boylan-Kolchin M., Bullock J. S., Lee K., 2014a, MNRAS, 438, 2578
Garrison-Kimmel S., Rocha M., Boylan-Kolchin M., Bullock J. S., Lally J., 2013, MNRAS, 433, 3539
Gorbunov D., Khmelnitsky A., Rubakov V., 2008, J. Cosmology Astropart. Phys., 0810, 041
Gritschneder M., Lin D. N. C., 2013, ApJ, 765, 38
Hahn O., Abel T., 2011, MNRAS, 415, 2101
Hazra D. K., Shafieloo A., Smoot G. F., Starobinsky A. A., 2014, J. Cosmology Astropart. Phys., 6, 61
Hinshaw G., et al., 2013, ApJS, 208, 19
Ho S., Cuesta A., Seo H.-J., de Putter R., Ross A. J., et al., 2012, ApJ, 761, 14
Horiuchi S., Humphrey P. J., Oñorbe J., Abazajian K. N., Kaplinghat M., Garrison-Kimmel S., 2014, Phys. Rev. D, 89, 025017
Hou Z., Reichardt C., Story K., Follin B., Keisler R., et al., 2014, ApJ, 782, 74
Kamionkowski M., Koushiappas S. M., Kuhlen M., 2010, Phys. Rev. D, 81, 043532
Kamionkowski M., Liddle A. R., 2000, Phys. Rev. Lett., 84, 4525
Kaplinghat M., 2005, Phys. Rev. D, 72, 063510
Katz N., White S. D. M., 1993, ApJ, 412, 455
Keeton C. R., Moustakas L. A., 2009, ApJ, 699, 1720
Klypin A., Kravtsov A. V., Valenzuela O., Prada F., 1999, ApJ, 522, 82
Knollmann S. R., Knebe A., 2009, ApJS, 182, 608
Kobayashi T., Takahashi F., 2011, J. Cosmology Astropart. Phys., 1, 26
Koch A., Kleyna J. T., Wilkinson M. I., Grebel E. K., Gilmore G. F., Evans N. W., Wyse R. F. G., Harbeck D. R., 2007, AJ, 134, 566
Kuhlen M., Diemand J., Madau P., 2008, ApJ, 686, 262
Lesgourgues J., Viel M., Haehnelt M., Massey R., 2007, J. Cosmology Astropart. Phys., 0711, 008
Liu H., Mertsch P., Sarkar S., 2014, ApJ, 789, L29
Lovell M. R., Frenk C. S., Eke V. R., Jenkins A., Gao L., Theuns T., 2014, MNRAS, 439, 300
Ludlow A. D., Navarro J. F., Angulo R. E., Boylan-Kolchin M., Springel V., Frenk C., White S. D. M., 2014, MNRAS, 441, 378
Martinez G. D., Bullock J. S., Kaplinghat M., Strigari L. E., Trotta R., 2009, J. Cosmology Astropart. Phys., 6, 14
Mateo M., Olszewski E. W., Walker M. G., 2008, ApJ, 675, 201
McDonald J., 2014, arXiv:1403.6650 [astro-ph]

Moore B., Ghigna S., Governato F., Lake G., Quinn T., Stadel J., Tozzi P., 1999, ApJ, 524, L19
Muñoz R. R. et al., 2005, ApJ, 631, L137
Murray S. G., Power C., Robotham A. S. G., 2013, Astronomy and Computing, 3, 23
Navarro J. F., Frenk C. S., White S. D. M., 1996, ApJ, 462, 563
Ng K. C. Y., Laha R., Campbell S., Horiuchi S., Dasgupta B., Murase K., Beacom J. F., 2014, Phys. Rev. D, 89, 083001
Ngan W. H. W., Carlberg R. G., 2014, ApJ, 788, 181
Oñorbe J., Garrison-Kimmel S., Maller A. H., Bullock J. S., Rocha M., Hahn O., 2014, MNRAS, 437, 1894
Oh S.-H., de Blok W., Brinks E., Walter F., Kennicutt, Robert C. J., 2011, AJ, 141, 193
Planck Collaboration et al., 2013, arXiv:1303.5076 [astro-ph]
Polisensky E., Ricotti M., 2011, Phys. Rev. D, 83, 043506
Polisensky E., Ricotti M., 2014, MNRAS, 437, 2922
Pontzen A., Governato F., 2012, MNRAS, 421, 3464
Pontzen A., Governato F., 2014, Nature, 506, 171
Robertson B. E. et al., 2013, ApJ, 768, 71
Sánchez-Conde M. A., Prada F., 2014, MNRAS, 442, 2271
Sawala T. et al., 2014, arXiv:1404.3724 [astro-ph]
Schneider A., Anderhalden D., Macciò A. V., Diemand J., 2014, MNRAS, 441, L6
Schultz C., Oñorbe J., Abazajian K. N., Bullock J. S., 2014, MNRAS, 442, 1597
Simon J. D., Bolatto A. D., Leroy A., Blitz L., Gates E. L., 2005, ApJ, 621, 757
Simon J. D., Geha M., 2007, ApJ, 670, 313
Somerville R. S., 2002, ApJ, 572, L23
Somerville R. S., Bullock J. S., Livio M., 2003, ApJ, 593, 616
Springel V., 2005, MNRAS, 364, 1105
Springel V. et al., 2008, MNRAS, 391, 1685
Strigari L. E., Koushiappas S. M., Bullock J. S., Kaplinghat M., Simon J. D., Geha M., Willman B., 2008, ApJ, 678, 614
Teyssier M., Johnston K. V., Kuhlen M., 2012, MNRAS, 426, 1808
Tinker J., Kravtsov A. V., Klypin A., Abazajian K., Warren M., Yepes G., Gottlöber S., Holz D. E., 2008, ApJ, 688, 709
Tollerud E. J., Boylan-Kolchin M., Barton E. J., Bullock J. S., Trinh C. Q., 2011, ApJ, 738, 102
Viel M., Becker G. D., Bolton J. S., Haehnelt M. G., 2013, Phys. Rev. D, 88, 043502
Walker M. G., Mateo M., Olszewski E. W., 2009, AJ, 137, 3100
Walker M. G., Penarrubia J., 2011, ApJ, 742, 20
Wan Y., Li S., Li M., Qiu T., Cai Y., Zhang X., 2014, Phys. Rev. D, 90, 023537
Wang J., Frenk C. S., Navarro J. F., Gao L., Sawala T., 2012, MNRAS, 424, 2715
Wang J., White S. D. M., 2007, MNRAS, 380, 93
Wolf J., Martinez G. D., Bullock J. S., Kaplinghat M., Geha M., Muñoz R. R., Simon J. D., Avedo F. F., 2010, MNRAS, 406, 1220
Zentner A. R., Bullock J. S., 2002, Phys. Rev. D, 66, 043003
Zentner A. R., Bullock J. S., 2003, ApJ, 598, 49
Zolotov A. et al., 2012, ApJ, 761, 71